QDROP: RANDOMLY DROPPING QUANTIZATION FOR EXTREMELY LOW-BIT POST-TRAINING QUANTIZATION

Anonymous authors
Paper under double-blind review

ABSTRACT

Recently, post-training quantization (PTQ) has driven much attention to produce efficient neural networks without long-time retraining. Despite the low cost, current PTQ works always fail under the extremely low-bit setting. In this study, we pioneeringly confirm that properly incorporating activation quantization into the PTQ reconstruction benefits the final accuracy. To deeply understand the inherent reason, a theoretical framework is established, which inspires us that the flatness of the optimized low-bit model on calibration and test data is crucial. Based on the conclusion, a simple yet effective approach dubbed as QDROP is proposed, which randomly drops the quantization of activations during reconstruction. Extensive experiments on various tasks including computer vision (image classification, object detection) and natural language processing (text classification and question answering) prove its superiority. With QDROP, the limit of PTQ is pushed to the 2-bit activation for the first time and the accuracy boost can be up to 51.49%. Without bells and whistles, QDROP establishes a new state of the art for PTQ.

1 INTRODUCTION

In recent years, deep learning has been applied to all walks of life and offered substantial convenience for people's production and activities. While the performance of deep neural networks continues to increase, the memory and computation cost also scale up fastly and bring new challenges for edge devices. Model compression techniques such as network pruning (Han et al., 2015), distillation (Hinton et al., 2015), network quantization (Jacob et al., 2018) and neural architecture search (Zoph & Le, 2016) etc., are dedicated to reducing calculation and storage overhead. In this paper, we study quantization which adopts low-bit representation for weights and activations to enable fixed-point computation and less memory space.

Based on the cost of a quantization algorithm, researchers usually divide the quantization work into two categories: (1) Quantization-Aware Training (QAT) and (2) Post-Training Quantization (PTQ). QAT finetunes a pre-trained model by leveraging the whole dataset and GPU effort. On the contrary, PTQ demands much less computation to obtain a quantized model since it does not require end-to-end training. Therefore, much attention has recently been paid to PTQ (Singh et al., 2019; Cai et al., 2020; Wang et al., 2020; Hubara et al., 2021; Banner et al., 2019; Nahshan et al., 2019; Zhang et al., 2021; Li et al., 2021b) due to its low cost and easy-to-use characteristics in practice.

Traditionally, PTQ pursues accuracy by performing the rounding-to-nearest operation, which focuses on minimizing the distance from the full-precision (FP) model in parameter space. In recent progress, Nagel et al. (2020); Li et al. (2021a) considered minimizing the distance in model space, i.e. the final loss objective. They use Taylor Expansion to analyze the change of loss value and derive a method to reconstruct the pre-trained model's feature by learning the rounding scheme. Such methods are efficient and effective in 4-bit quantization and can even push the limit of weight quantization to 2-bit. However, the extremely low-bit activation quantization, which faces more challenges, still fails to achieve satisfactory accuracy. We argue that one key reason is that existing theoretical analyses only model the weight quantization as perturbation while ignoring activation's. This will lead to the same optimized model no matter which bit the activations use, which is obviously counter-intuitive and thus causes a sub-optimal solution.

In this work, the effect of activation quantization in PTQ is deeply investigated for the first time. We empirically observe that perceiving the activation quantization benefits the extremely low-bit PTQ reconstruction and surprisingly find that only partial activation quantization is more preferable. An intuitive understanding is that incorporating activation will lead to a different optimized weight. Inspired by this, we conduct theoretical studies on how activation quantization affects the weight tuning, and the conclusion is that involving activation quantization into the reconstruction helps the flatness of model on calibration data and dropping partial quantization contributes to the flatness on test data. Motivated by both empirical and theoretical findings, we propose QDROP that randomly drops quantization during the PTQ reconstruction to pursue the flatness from a general perspective. With this simple and effective approach, we set up a new state of the art for PTQ on various tasks including image classification, object detection for computer vision, and text classification and question answering for natural language processing.

This paper makes the following contributions:

1. We confirm the benefits unprecedentedly from involving activation quantization in the PTQ reconstruction and surprisingly observe that partial involvement of activation quantization performs better than the whole.
2. A theoretical framework is established to deeply analyze the influence of incorporating activation quantization into weight tuning. Using this framework, we conclude that the flatness of the optimized low-bit model on calibration data and test data are crucial for the final accuracy.
3. Based on the empirical and theoretical analyses, we propose a simple yet effective method QDROP that achieves the flatness from a general perspective. QDROP is easy to implement and can consistently boost existing methods as a plug-and-play module for various neural networks including CNNs like ResNets and Transformers like BERT.
4. Extensive experiments on a large variety of tasks and models prove that our method set up a new state of the art for PTQ. With QDROP, the 2-bit post-training quantization becomes possible for the first time.

2 RELATED WORKS

Post-training quantization Rounding-to-nearest operation is known to be the direct and easy way for quantizing parameters or activations in PTQ. Although there is almost no accuracy drop when quantizing to 8-bit, lower bit quantization is yet a hard task and worth exploring. (Choukroun et al., 2019) transforms quantization to a Minimum Mean Squared Error problem both for weights and activations. (Singh et al., 2019) equalizes weight ranges among channels thus be more favorable to per-layer quantization and employs bias correction to absorb the output error induced by quantization. However, such methods neglect the task loss thus lead to a sub-optimal. AdaRound (Nagel et al., 2020), which proposes to learn the rounding mechanism by reconstructing output layer by layer brings more opportunities for 4-bit quantization. Besides layer reconstruction, BRECQ (Li et al., 2021a) discusses more choices and advises to do block reconstruction with better accuracy at 2-bit weight quantization. Nonetheless, we argue that AdaRound and BRECQ isolate weight quantization and activation one theoretically and experimentally, which might be a key point of failures on extremely low-bit quantization.

Flatness The idea of "flat" minima might date back to (Hochreiter & Schmidhuber, 1997), where the benefits are recognized in recent years, such as generalization (Jiang et al., 2019; Keskar et al., 2016) and adversarial training (Wu et al., 2020; Zheng et al., 2021). Some previous works (Izmailov et al., 2018; Foret et al., 2020) devote to improve the flatness of the trained weight for robustness under perturbation or distribution shift. Other ideas try to model flatness or sharpness formally by visualization of loss landscape or mathematical formulas. And for quantization, which could be viewed as some kind of noise, a flat model has been implied to be preferable, (Dong et al., 2019; Yang et al., 2019; Kadambi et al., 2020). Despite the natural fact that flatness helps with weight quantization, how does activation quantization involves with smoother loss surface has not been discussed deeply, particularly for post-training quantization.

3 PRELIMINARIES

Basic Notations. Throughout this paper, matrices (or tensors) are marked as $\boldsymbol{X}$, whereas the vectors are denoted by $\boldsymbol{x}$. Sometimes we use $\boldsymbol{w}$ to represent the flattened version of the weight

matrix $\boldsymbol{W}$. For a feedforward neural network with ReLU or identity activation function, we denote it as $\mathcal{G}(\boldsymbol{x}, \boldsymbol{w})$ and the loss function as $L(\boldsymbol{x}, \boldsymbol{w})$, where $\boldsymbol{x}$ and $\boldsymbol{w}$ are the network inputs and weights, respectively. Note that we assume $\boldsymbol{x}$ is sampled from training dataset $\mathcal{D}_t$, thus the final loss is denoted by $\mathbb{E}_{\boldsymbol{x}\sim\mathcal{D}_t}[L(\hat{\boldsymbol{w}}, \boldsymbol{x})]$. For the network forward function, we can write it as:

$$\boldsymbol{z}_j^{(\ell+1)} = \sum_i \boldsymbol{W}_{i,j}^{(\ell)} \boldsymbol{a}_i^{(\ell)}, \quad f(\boldsymbol{z}_j^{(\ell+1)}) = \boldsymbol{a}_j^{(\ell+1)}. \tag{1}$$

where w_{ij} denotes weight connecting the ith activation neuron and the jth output. The bracket superscript (ℓ) is the layer index. $f(\cdot)$ indicates the activation function.

Post-training Quantization. Uniform quantizer maps continuous values $x \in \mathbb{R}$ into fixed-point integers. For instance, the activation quantization function can be written as $\hat{x} = \lfloor \frac{x}{s} \rceil s$, where $\lfloor \cdot \rceil$ denotes the rounding-to-nearest operator, s is the step size between two subsequent quantization levels. While rounding-to-nearest operation minimizes the mean squared error between $\hat{X}$ and x, the minimization of parameter space certainly cannot equal to the minimization in final task loss (Li et al., 2021a), i.e., $\mathbb{E}_{\boldsymbol{x}\sim\mathcal{D}_t}[L(\hat{\boldsymbol{w}}, \boldsymbol{x})]$. However, in the post-training setting, we only have a tiny subset $\mathcal{D}_c \in \mathcal{D}_t$ that only contains 1k images. Thus, it is hard to minimize the final loss objective with limited data.

Recently, a series of works (Nagel et al., 2020; Li et al., 2021a) learn to either round up or down and view the new rounding mechanism as weight perturbation, i.e., $\hat{\boldsymbol{w}} = \boldsymbol{w} + \Delta\boldsymbol{w}$. Take a pre-trained network $\mathcal{G}$ as an example, they leverage Taylor Expansion to analyze the target, which reveals the quantization interactions among weights:

$$\min_{\hat{\boldsymbol{w}}} \mathbb{E}\left[L(\boldsymbol{x}, \hat{\boldsymbol{w}}) - L(\boldsymbol{x}, \boldsymbol{w})\right] \approx \min_{\hat{\boldsymbol{w}}} \mathbb{E}\left[\frac{1}{2}\Delta\boldsymbol{w}^\top \mathbf{H}^{\boldsymbol{w}} \Delta\boldsymbol{w}\right], \tag{2}$$

where $\mathbf{H}_{\boldsymbol{w}} = \mathbb{E}_{\boldsymbol{x}\sim\mathcal{D}_t} \nabla^2_{\boldsymbol{w}} L(\boldsymbol{w}, \boldsymbol{x})$ is the expected second-order derivative. The above objective could be transformed into the change of output weighted by the output Hessian.

$$\min_{\hat{\boldsymbol{w}}} \mathbb{E}\left[\Delta\boldsymbol{w}^\top \mathbf{H}^{\boldsymbol{w}} \Delta\boldsymbol{w}\right] \approx \min_{\hat{\boldsymbol{w}}} \mathbb{E}\left[\Delta\boldsymbol{a}^\top \mathbf{H}^{\boldsymbol{a}} \Delta\boldsymbol{a}\right] \tag{3}$$

About the above minimization, they **finetune only the weight** by reconstructing each block/layer output (See Figure 1(a)). But they did not explore the activation quantization during output reconstruction with only modeling weight quantization as noise. The step size for activation quantization is determined after the reconstruction stage.

Intuitively, when quantizing the activations of a full-precision model to 2-bit and 3-bit, there should be different suitable weights. However, the existing works result in the same optimized weight due to the neglect of activation quantization. Therefore, we argue that when quantizing the neural network, the noise caused by activation quantization should be considered coherently with weights.

4 METHODOLOGY

In this section, to reveal the influence of introducing activation quantization before output reconstruction, we first conduct empirical experiments and present two observations. Then a theoretical framework is built to investigate how the activation quantization affects the optimized weights. Last, equipped with the analysis conclusions, a simple yet effective method dubbed QDROP is proposed.

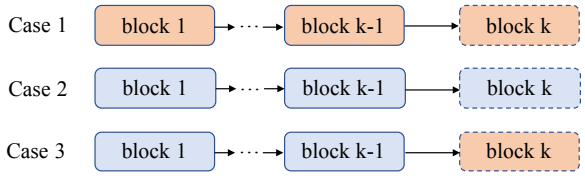

Figure 1: 3 cases to involve activation quantization when optimizing the k_{th} block's weight rounding. Activations are quantized inside the blue block and not quantized inside the orange block.

Case	1	2	3
ResNet-18	31.26	50.86	52.83
ResNet-50	9.52	51.90	53.42
MobileNet-V2	4.88	37.85	38.51
RegNet-600MF	2.86	27.69	31.92
MnasNet	14.63	48.12	49.40

Table 1: 2-bit post-training quantization accuracy on ImageNet dataset, given different cases and different network models.

4.1 EMPIRICAL OBSERVATIONS

To investigate the influence of activation quantization when reconstructing the layer/block output, we conduct preliminary experiments on the ImageNet (Russakovsky et al., 2015) dataset. Our experiments are based on the open-sourced code Li et al. (2021a) except that we will introduce activation quantization from 1 to $k-1$ blocks before the k_{th} block's reconstruction. We give a simple visualization in Fig. 1 to show 3 cases for putting activation quantization in different stages. Case 1 means that all activation are kept in 32-bit full-precision during the reconstruction of block output, which is also adopted in existing work Nagel et al. (2020); Li et al. (2021a). Case 2 and Case 3 are used for incorporating activation quantization into the reconstruction stage. However, Case 3 will omit the current block's quantization while Case 2 will not. The detailed results of these three cases are listed in Table 1 and the algorithm is put in algorithm 2.

According to the comparison, we can obtain two observations:

1. *For extremely low-bit quantization (e.g., W2A2), there will be huge accuracy improvement when considering activation quantization during weight tuning.* This is confirmed by comparing with Case 1 and Case 2. We find Case 1 barely converges while Case 2 achieves good accuracy. It reveals that a separate optimization of weights and activations cannot find an optimal solution. After introducing the activation quantization, the weights will learn to diminish the influence of activation quantization.
2. *Partially introducing block-wise activation quantization surpasses introducing the whole activation quantization.* Case 3 does not quantize the activations inside the current tuning block but achieves better results than Case 2. This inspires us that how much quantization of activations we introduce will affect the final accuracy.

4.2 HOW DOES ACTIVATION QUANTIZATION AFFECT WEIGHT TUNING

The empirical observations have highlighted the importance of activation quantization during the PTQ pipeline. To further explore how activation quantization will affect the weight tuning, we build a theoretical framework that analyzes the final loss objective with both weights and activations being quantized, which presents clues of high accuracy for extremely low-bit post-training quantization.

Conventionally, the activation quantization could be modeled as injecting some form of noise imposed on the full-precision counterpart, defined as $e = (\hat{a} - a)$. Here we translate the noise into a scaling form, i.e., $\hat{a} = a \cdot (1 + u)$, for the ease of understanding the later theoretical analyses.

Equipped with the activation noise, we define our optimization objective in PTQ as:

$$\min_{\hat{\boldsymbol{w}}} \mathbb{E}_{\boldsymbol{x}\sim\mathcal{D}_c}[L(\boldsymbol{w} + \Delta\boldsymbol{w}, \boldsymbol{x}, \mathbf{1} + \boldsymbol{u}(\boldsymbol{x})) - L(\boldsymbol{w}, \boldsymbol{x}, \mathbf{1})]. \tag{4}$$

Note that we add another argument in calculating the loss function, which is the noise on activation. Also, we use $\mathbf{1} + \boldsymbol{u}(\boldsymbol{x})$ to denote such noise since it is related to specific input data point $\boldsymbol{x}$. We hereby use a transformation that can absorb the noise on activation. Consider a simple matrix-vector multiplication $\boldsymbol{W}\boldsymbol{a}$, we have $\boldsymbol{W}(\boldsymbol{a} \odot (\mathbf{1} + \boldsymbol{u}(\boldsymbol{x}))) = (\boldsymbol{W} \odot (\mathbf{1} + \boldsymbol{V}(\boldsymbol{x})))\boldsymbol{a}$, given by

$$\boldsymbol{W}(\begin{bmatrix} 1+\boldsymbol{u}_1(\boldsymbol{x}) \\ 1+\boldsymbol{u}_2(\boldsymbol{x}) \\ \dots \\ 1+\boldsymbol{u}_n(\boldsymbol{x}) \end{bmatrix} \odot \boldsymbol{a}) = (\begin{bmatrix} 1+\boldsymbol{u}_1(\boldsymbol{x}) & 1+\boldsymbol{u}_1(\boldsymbol{x}) & \dots & 1+\boldsymbol{u}_1(\boldsymbol{x}) \\ 1+\boldsymbol{u}_2(\boldsymbol{x}) & 1+\boldsymbol{u}_2(\boldsymbol{x}) & \dots & 1+\boldsymbol{u}_2(\boldsymbol{x}) \\ \dots \\ 1+\boldsymbol{u}_n(\boldsymbol{x}) & 1+\boldsymbol{u}_n(\boldsymbol{x}) & \dots & 1+\boldsymbol{u}_n(\boldsymbol{x}) \end{bmatrix} \odot \boldsymbol{W})\boldsymbol{a}, \tag{5}$$

where the $\mathbf{1}+\boldsymbol{u}(\boldsymbol{x})$ is the scaled factor of activation quantization. This simple equation can transplant the noise on the activation vector into weight matrix, where for a specific input data point $\boldsymbol{x}$, there are two distinct $\boldsymbol{u}(\boldsymbol{x})$ and $\boldsymbol{v}(\boldsymbol{x})$. Also note that for a convolution layer, we cannot apply such transformation since the input to convolution is a matrix and will cause different $\boldsymbol{V}$. Nonetheless, we can give a formal lemma that absorbs $\boldsymbol{u}$ (see the Appendix Appendix A for rigorous proof):

Lemma 1. *For a quantized (convolutional) neural network, the influence of activation quantization on the final loss objective in post-training quantization can be transformed into weight perturbations.*

$$\mathbb{E}_{\boldsymbol{x}\sim\mathcal{D}_c}[L(\hat{\boldsymbol{w}}, \boldsymbol{x}, \mathbf{1} + \boldsymbol{u}(\boldsymbol{x})) - L(\boldsymbol{w}, \boldsymbol{x}, \mathbf{1})] \approx \mathbb{E}_{\boldsymbol{x}\sim\mathcal{D}_c}[L(\hat{\boldsymbol{w}} \odot (\mathbf{1} + \boldsymbol{v}(\boldsymbol{x})), \boldsymbol{x}) - L(\boldsymbol{w}, \boldsymbol{x})] \tag{6}$$

By interpolating $L(\hat{\boldsymbol{w}}, \boldsymbol{x})$ into Lemma 1, we can obtain the final theorem:

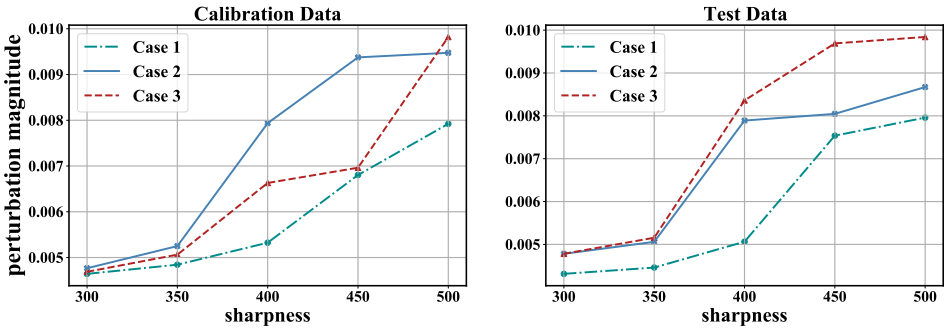

Figure 2: Measure sharpness on different data distributions among three cases. We adopt the measurement defined in (Keskar et al., 2016). With the same degree of loss change ratio, those who can tolerate a larger perturbation magnitude enjoy a flatter loss landscape.

Theorem 1. *For a neural network $\mathcal{G}$ with quantized weight $\hat{\boldsymbol{w}}$ and activation perturbation scale $\mathbf{1}+\boldsymbol{u}(\boldsymbol{x})$, we have:*

$$\mathbb{E}_{\boldsymbol{x}\sim\mathcal{D}_c}[L(\hat{\boldsymbol{w}},\boldsymbol{x},\mathbf{1}+\boldsymbol{u}(\boldsymbol{x}))-L(\boldsymbol{w},\boldsymbol{x},\mathbf{1})]\approx \mathbb{E}_{\boldsymbol{x}\sim\mathcal{D}_c}[\underbrace{(L(\hat{\boldsymbol{w}},\boldsymbol{x})-L(\boldsymbol{w},\boldsymbol{x}))}_{(7-1)}+\underbrace{(L(\hat{\boldsymbol{w}}\odot(1+\boldsymbol{v}(\boldsymbol{x})),\boldsymbol{x})-L(\hat{\boldsymbol{w}},\boldsymbol{x}))}_{(7-2)}] \tag{7}$$

Here, Theorem 1 divides optimization objective into two terms. Term (7-1) is the same as Eq. (2) explored in (Nagel et al., 2020; Li et al., 2021a), which reveals how weight quantization interacts with loss function. Term (7-2) is the loss change by adding activation quantization on the weight quantized network $\mathcal{G}(\hat{\boldsymbol{w}},\boldsymbol{x})$.

In another way to interpret Eq. (7), the term (7-2) stands for the loss change with jitters on the quantized weight. This type of noise correlates with certain kinds of robustness. As stated in some works about generalization and flatness (Dinh et al., 2017; Hochreiter & Schmidhuber, 1997), the intuitive understanding of so-called flat minimal means the loss of connected region around the minimal is relatively similar and (Neyshabur et al., 2017) defines and optimizes an "expected sharpness", i.e, $\mathbb{E}_{\boldsymbol{v}}[\hat{L}(f_{\boldsymbol{w}+\boldsymbol{v}})]-\hat{L}(f_{\boldsymbol{w}})$, to improve the converged flatness after training. From this perspective, the term (7-2) can be interpreted as some kind of flatness, and thereby we could achieve the following corollary.

Corollary 1. *With activation quantization, the trained quantized weights are usually flatter on some directions and more robust under some perturbations for calibration data.*

With Corollary 1, Case 2 and 3 discussed in Sec. 4.1 enjoy a flatter loss landscape benefited from perceiving the activation quantization. This explains their superiority compared with Case 1. The measurement of sharpness on calibration data (left part) in Fig. 2 further validates this point. With similar perturbation magnitude, Case 2 and 3 suffer less loss degradation than Case 1.

4.3 QDROP

As aforementioned, introducing activation quantization is theoretically proved to produce a flatter model than existing works and the directions of flatness depend on the data distribution. Since the PTQ is especially sensitive to calibration data (Yu et al., 2021), we need to transfer the investigations in Sec. 4.2 on calibration data into the test setting for a thorough understanding. In specific, we consider Eq. (7) in test set and inspect two terms separately in the following. Based on the analyses, our method QDROP will be derived to pursue an excellent performance on test data.

Term (7-1) on test set. As suggested in Sec. 4.2, with both quantized activations and weights, we additionally optimize the term (7-2) representing the flatness on calibration data. This term will encourage the quantized model to learn a flat minimum. As a result, the traditional objective of AdaRound (term (7-1)) can naturally generalize better for test data (i.e., $\mathbb{E}_{\boldsymbol{x}\sim\mathcal{D}_t}\left(L(\hat{\boldsymbol{w}},\boldsymbol{x})-L(\boldsymbol{w},\boldsymbol{x})\right)$).

Algorithm 1: QDROP in one block for one batch

Input: the k_{th} block from layer i to layer j, a minibatch of quantized block input $\hat{\boldsymbol{a}}^{i-1}$, FP32 block input $\boldsymbol{a}^{i-1}$, FP32 block output $\boldsymbol{a}^{j}$, quantization dropping probability p.

{1. Forward propagation:}

Substitute $\hat{\boldsymbol{a}}^{i-1}$ with corresponding $\boldsymbol{a}^{i-1}$ at neuron-level with probability p and mark the replaced input as $\tilde{\boldsymbol{a}}^{i-1}$;

for $l = i$ *to* j **do**

  $\boldsymbol{a}^{l} \leftarrow \boldsymbol{W}^{l}\tilde{\boldsymbol{a}}^{l-1}$;

  $\hat{\boldsymbol{a}}^{l} \leftarrow$ Quantize($\boldsymbol{a}^{l}$);

  randomly drop some $\hat{\boldsymbol{a}}^{l}$ with $\boldsymbol{a}^{l}$ as defined in Eq. (9) and get $\tilde{\boldsymbol{a}}^{l}$;

{2. Backward propagation:}

Compute $\Delta\boldsymbol{a}^{j} = \tilde{\boldsymbol{a}}^{j} - \boldsymbol{a}^{j}$;

Tune the weight by gradient descent ;

return Quantized block ;

Term (7-2) on test set. Furthermore, we should also concern about the term (7-2) on test data, i.e. $\mathbb{E}_{\boldsymbol{x}\sim\mathcal{D}_t}[L(\hat{\boldsymbol{w}} \odot (\mathbf{1} + \boldsymbol{v}(\boldsymbol{x})), \boldsymbol{x}) - L(\hat{\boldsymbol{w}}, \boldsymbol{x})]$. As revealed in Sec. 4.2, the term (7-2) implies the flatness where its situation on calibration data has been exploited. Here, we further investigate the flatness on test samples. Fig. 2 shows that there is a gap between the test data and calibration data for the flatness of the 3 cases. According to Corollary 1, these 3 cases in fact introduce different $\boldsymbol{u}$ mathematically and thus will result in different flatness directions, given by:

$$\text{Case 1: } \boldsymbol{u} = \mathbf{0};\ \text{Case2: } \boldsymbol{u} = \frac{\hat{\boldsymbol{a}}}{\boldsymbol{a}} - 1;\ \text{Case 3: } \boldsymbol{u} = \begin{cases} \frac{\hat{\boldsymbol{a}}}{\boldsymbol{a}} - 1, & \text{block}_1 \sim \text{block}_{k-1} \\ \mathbf{0}, & \text{block}_k \end{cases} \tag{8}$$

For Case 1, there is no activation quantization during calibration without taking flatness into account. Case 2 suggests the activation perturbation totally and therefore enjoys a good flatness on calibration data. However, due to the mismatch on calibration data and test one, it is highly possible that Case 2 causes overfitting. Case 3, in fact achieves the best performance by dropping some activation quantization along with diverse weight perturbations. This inspires us to pursue a flat minimum from a general perspective, that only optimizing the target on calibration set is suboptimal to test set.

QDROP. Inspired by this, we propose QDROP to further increase the flatness on as many directions as possible. In particular, we randomly disable and enable the quantization of the activation:

$$\text{QDROP}: u = \begin{cases} 0 & \text{with probability } p \\ \frac{\hat{a}}{a} - 1 & \text{with probability } 1 - p \end{cases}. \tag{9}$$

We name it QDROP because it randomly drops the quantization of activation. It is a fine-grained version of Case 3 since Case 3 drops the quantization in a block-wise manner, whereas our QDROP operates in an element-wise way. Theoretically, QDROP can introduce different directions of noise. That is to say, different and random $\boldsymbol{u}$ can diversify the directions of flatness, which contributes to the final high accuracy.

Discussions. QDROP can be viewed as a generalized form of the existing schemes. Case 1 and 2 respectively corresponds to the dropping probability of $p = 1$ and $p = 0$. Case 3 is equivalent to setting the block being optimized with dropping probability $p = 1$ and remains the quantization of other parts. Note that the p obeys Bernoulli distribution and thus can be set as 0.5 for the maximal entropy (Qin et al., 2020), which is helpful for flatness across various directions.

QDROP is easy to implement for various neural networks including CNNs and Transformers, and plug-and-play with little additional computational complexity. With QDROP, the complicated problem of choosing optimization order, i.e. different cases in Sec. 4.1, can be avoided. Besides, the established theoretical framework is general and can be applied to analyze and explain why some existing methods that aim to improve the flatness of full-precision model also performs well (details refer to Sec. B.2).

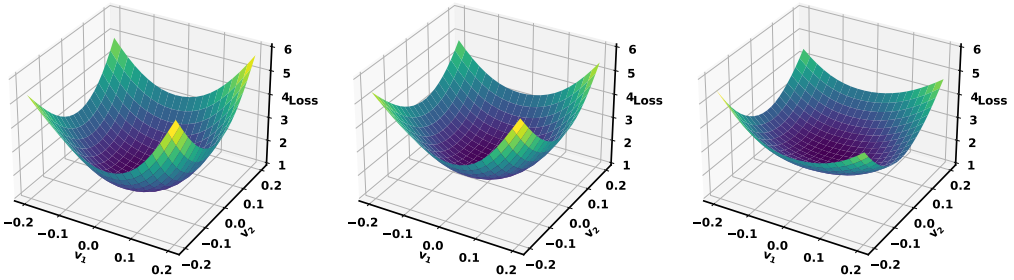

(a) Case 1 (b) Case 3 (c) QDROP

Figure 3: Loss surface of the quantized weight for QDROP, Case 1 and 3 on test data and ResNet-18 W3A3.

Method	Bits (W/A)	ResNet-18	ResNet-50	MobileNetV2	RegNet-600MF	RegNet-3.2GF	MNasNet-2.0
No Drop	2/2	51.19	52.59	5.86	28.95	40.98	16.482
QDROP	2/2	**54.72**	**58.67**	**13.05**	**41.49**	**55.11**	**28.77**
No Drop	2/3	62.03	66.76	38.06	55.38	65.08	47.612
QDROP	2/3	**62.91**	**68.11**	**42.75**	**58.40**	**68.00**	**55.80**

Table 2: Effect of QDROP.

5 EXPERIMENTS

In this section, we conduct two sets of experiments to verify the effectiveness of QDROP. In Sec. 5.1, we first conduct an ablation study for the impact with and without dropping quantization and analyze the option of distinct quantization dropping rates. In Sec. 5.2, we compare our method with other existing approaches across vision and language tasks.

Implementation Details. Our code is based on PyTorch Paszke et al. (2019), and has been attached in our supplemental material. We set the default dropping probability p as 0.5, except we explicitly mention it. Our experiments including image classification on ImageNet, object detection on MS COCO, and natural language processing on GLUE benchmark and SQuAD. The weight tuning method is the same with Nagel et al. (2020); Li et al. (2021a). Each block or layer output is reconstructed for 20k iterations. For ImageNet dataset, we sample 1024 images as calibration set, while COCO we use 256 images. In NLP, we sample 1024 examples. We also keep the first and the last layer in 8-bit and adopt per-channel weight quantization. We use W4A4 to represent 4-bit weight and activation quantization. More model choices and other settings is described in Appendix C.

5.1 ABLATION STUDY

Effect of QDROP. We propose QDROP and here we would like to test the effect of PTQ with or without QDROP. We use ImageNet classification benchmark and quantize the weight parameters to 2-bit and quantize activation to 2/3-bit. As shown in Table 2, QDROP improves the accuracy across all bit settings evaluated for 6 models on ImageNet. Furthermore, the gains are more obvious when applying QDROP to lightweight network architecture: 4.69% increment for MobileNet-V2 under W2A3 and 14.13% for RegNet-3.2GF with W2A2.

Effect of Dropping Probability. We also explore the dropping probability in PTQ. We choose p in [0,0.25,0.5,0.75,1] and test on ResNet-50 and MobileNetV2. The results are summarized in Fig. 5. We find 0.5 generally performs best among 5 candidates. Although there could be a fine-grained best solution for each architecture. We shall avoid cumbersome hyper-parameter search and continue using 0.5.

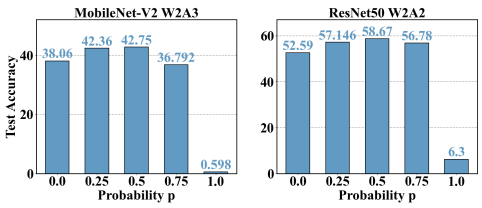

Figure 5: Impact of dropping probability on ImageNet.

Methods	Bits (W/A)	ResNet-18	ResNet-50	MobileNetV2	RegNet-600MF	RegNet-3.2GF	MNasNet-2.0
Full Prec.	32/32	71.08	77.00	72.49	73.71	78.36	76.68
ACIQ-Mix (Banner et al., 2019)	4/4	67.00	73.80	-	-	-	-
ZeroQ (Cai et al., 2020)*	4/4	21.71	2.94	26.24	28.54	12.24	3.89
LAPQ (Nahshan et al., 2019)	4/4	60.30	70.00	49.70	57.71*	55.89*	65.32*
AdaQuant (Hubara et al., 2021)	4/4	69.60	**75.90**	47.16*	-	-	-
Bit-Split (Wang et al., 2020)	4/4	67.56	73.71	-	-	-	-
AdaRound (Nagel et al., 2020)*	4/4	69.36	74.76	64.33	-	-	-
BRECQ (Li et al., 2021a)	4/4	69.60	75.05	66.57	68.33	74.21	73.56
QDROP (Ours)	4/4	**69.62**	75.45	**68.84**	**71.18**	**76.66**	**73.71**
LAPQ (Nahshan et al., 2019)*	2/4	0.18	0.14	0.13	0.17	0.12	0.18
AdaQuant (Hubara et al., 2021)*	2/4	0.11	0.12	0.15	-	-	-
AdaRound (Nagel et al., 2020)*	2/4	64.14	68.40	41.52	59.27	65.33	53.77
BRECQ (Li et al., 2021a)	2/4	64.80	70.29	53.34	59.31	67.15	63.01
QDROP (Ours)	2/4	**65.25**	**70.65**	**54.22**	**63.80**	**71.70**	**64.24**
AdaRound (Nagel et al., 2020)*	3/3	64.66	66.66	15.20	51.01	56.79	47.89
AdaQuant (Hubara et al., 2021)*	3/3	60.09	67.46	2.23	-	-	-
BRECQ (Li et al., 2021a)*	3/3	65.87	68.96	23.41	55.16	57.12	49.78
QDROP (Ours)	3/3	**66.75**	**72.38**	**57.98**	**65.54**	**72.51**	**66.81**
BRECQ (Li et al., 2021a)*	2/2	42.54	29.01	0.24	3.58	3.62	0.61
QDROP (Ours)	2/2	**54.72**	**58.67**	**13.05**	**41.47**	**55.11**	**28.77**

Table 3: Comparison among different post-training quantization strategies with low-bit activation in terms of accuracy on ImageNet. * represents for our implementation according to open-source codes and we apply the same settings such as per-channel weight quantization.

5.2 LITERATURE COMPARISON

ImageNet. We choose ResNet-18 and -50 (He et al., 2016), MobileNetV2 (Sandler et al., 2018) in ImageNet comparison. Besides these common architectures, we also compare the searched MNasNet (Tan et al., 2019) and RegNet (Radosavovic et al., 2020). Some baseline methods do not report the low bit cases, therefore we implement them based on the open-source codes with unified settings. We summarize the results in Table 3. First, the W4A4 quantization is investigated. It can be observed that QDROP provides $0 \sim 3\%$ accuracy uplift when compared to strong baselines including AdaRound, BRECQ, AdaQuant. With W2A4 quantization, QDROP can improve the accuracy of ResNet-50 by 0.5%, and RegNet-3.2GF by 4.6%. In addition, to fully exploit the limit of QDROP, we conduct more challenging cases which quantize the weights and activations to 2 or 3 bits. According to the last two rows of Table 3, our proposed QDROP consistently achieves good results while existing methods suffer from non-negligible accuracy drop. In W3A3 quantization, our method can quantize ResNet-50 to 72.4% accuracy while the best existing work only has 69% accuracy. On MobileNetV2, the difference is even larger, where our method reaches 58% accuracy and BRECQ only gets 23%. In the W2A2 setting, the PTQ becomes much harder. QDROP outperforms the competing method by a large margin: 12.18% upswings for ResNet-18, 29.66% for ResNet-50 and 51.49% for RegNet-3.2GF.

MS COCO. In this part, we validate the performance of QDROP on object detection task using MS COCO dataset. We use both two-stage Faster RNN (Ren et al., 2015) and one-stage RetinaNet (Lin et al., 2017) models. Backbone are selected from ResNet-18, ResNet-50, and MobileNetV2. Note that we set the first layer and the last layer to 8-bit and do not quantize the head of the model, however, the neck (FPN) is quantized. Experiments show that W4A4 quantization using QDROP nearly do not affect Faster RCNN's mAP. For RethinaNet, our method has 5 mAP improvement on MobileNetV2 backbone. In low bit setting W2A4, our method shows great improvement both on Faster-RCNN and RetinaNet, up to 6.5 mAP.

GLUE benchmark and SQuAD. Transformer has made significant progress in the language processing field. And Bert, as a representative baseline in NLP, is getting larger and many compression works have been proposed. We test QDROP in NLP tasks including the GLUE benchmark and SQuAD1.1. They are all conducted on the typical NLP model, i.e, BERT (Devlin et al., 2018). Compared with those QAT methods (Zafrir et al., 2019; Bai et al., 2020), which usually adopt data augmentation trick to achieve dozens of times the original data, we only randomly extract 1024 examples without any extra data processing and quantize all the parts of BERT while some works (Zafrir et al., 2019) ignore quantization of attention probability. Besides AdaQuant and BRECQ, which suffer a huge accuracy degradation, our QDROP surpasses No QDROP all the tasks, specifically on QNLI(8.7%), QQP(4.6%) and RTE(7.2%). As for SST-2, despite little enhancement by

Method	Bits (W/A)	Faster RCNN			RetinaNet		
		ResNet-18	ResNet-50	MobileNet-V2	ResNet-18	ResNet-50	MobileNet-V2
Full Prec.	32/32	34.60	38.56	33.47	33.22	36.80	32.63
AdaRound*	4/4	32.57	34.47	26.11	31.04	33.51	24.99
BRECQ*	4/4	32.58	34.59	26.58	31.21	33.47	24.84
QDROP	4/4	**33.37**	**36.96**	**30.88**	**31.99**	**35.67**	**29.75**
AdaRound*	2/8	30.54	33.15	25.35	29.30	32.22	24.22
BRECQ	2/8	31.82	34.23	27.54	**31.42**	34.75	**27.59**
QDROP	2/8	**32.20**	**36.14**	**28.48**	31.03	**34.84**	27.42
BRECQ*	2/4	29.92	30.23	19.35	28.73	29.47	18.46
QDROP	2/4	**31.01**	**34.23**	**25.04**	**29.69**	**33.01**	**24.89**

Table 4: Comparison among typical post-training quantization strategies in terms of mAP on MS COCO. Note that refer to BRECQ, we didn't quantize head and keep the first and last layer in backbone to 8-bit. Other notations align the upper table.

Method	SST-2 (acc)	QNLI (acc)	QQP (f1/acc)	STS-B (Pearson/Spearman corr)	MNLI (acc m/mm)	MRPC (acc)	RTE (acc)	CoLA (Matthews corr)	SQuAD1.1 (f1)
Full Prec.	92.43	91.54	87.81/90.91	88.04/ 87.63	84.57/84.46	87.71	72.56	53.39	88.42
AdaQuant*	-	-	-	-	-	-	-	-	5.17
BRECQ*	50.86	50.72	4.47/62.28	5.94/ 6.39	31.91/31.81	31.69	52.34	0.946	68.58
QDROP$_{1.0}$	87.94	68.05	68.09/76.69	82.24/81.68	69.19/71.28	77.39	53.43	40.17	75.97
QDROP	**88.06**	**76.75**	**72.66/79.04**	**82.39/81.88**	**71.43/73.70**	**79.15**	**60.65**	**40.85**	**77.26**

Table 5: Performance on NLP tasks compared to other methods on $E8W4A4$. Here, we use symbol $EeWwAa$ to additionally express the embedding bit and conduct experiments on GLUE and SQuAD1.1.

dropping quantization, it is indeed close to the FP32 value within 4.4%. And for STS-B, we argue that the origin fine-tuned model is trained with limited data, which might not be very representative to show the power of our method.

5.3 ROBUSTNESS OF QDROP

In this part, we discuss the effectiveness of QDROP under more challenging situations including even less data and cross-domain ones. Concerning about size of calibration data, we consider another 4 options. It can be observed that dropping some quantization behaves better under each setting and is even comparable with No QDROP with half of the original calibration data. Motivated by Yu et al. (2021), we also reconstruct block output by 1024 examples from out-of-domain data, i.e, CIFAR100 (Krizhevsky et al., 2009), MS COCO, and test on ImageNet. Results are available in Fig. 5.3, where our QDROP still works steadily. It is worth noting that on MS COCO W4A4, it actually reaches the accuracy from calibrating by in-domain data with and without dropping quantization, which implies the similar data distribution between MS COCO and ImageNet.

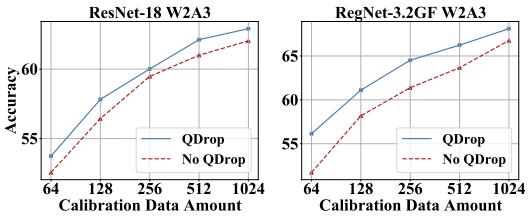

Figure 6: Impact of calibration data size on ImageNet

Calibration	Bits (W/A)	No QDROP	QDROP
MS COCO	4/4	69.49	**69.60**
MS COCO	3/3	65.642	**66.444**
CIFAR100	4/4	56.656	**60.340**
CIFAR100	3/3	27.940	**39.716**

Table 6: Cross domain data

6 CONCLUSION

In this paper, we have introduced QDROP, a novel mechanism for post-training quantization. QDrop aims to achieve good test accuracy given a tiny calibration set. This is done by optimization towards a flat minima. We dissect the PTQ objective theoretically into a flatness problem and improve the flatness from a general perspective. QDROP is easy to implement, computationally fast, and can be combined with existing methods to achieve further improvement. We comprehensively verify the effectiveness of QDROP on a large variety of tasks. It can achieve a nearly lossless 4-bit quantized network and can significantly improve the 2-bit quantization results, establishing a new state of the art for post-training quantization.

REFERENCES

Haoli Bai, Wei Zhang, Lu Hou, Lifeng Shang, Jing Jin, Xin Jiang, Qun Liu, Michael Lyu, and Irwin King. Binarybert: Pushing the limit of bert quantization. *arXiv preprint arXiv:2012.15701*, 2020.

Ron Banner, Yury Nahshan, and Daniel Soudry. Post training 4-bit quantization of convolutional networks for rapid-deployment. In *Advances in Neural Information Processing Systems*, 2019.

Yaohui Cai, Zhewei Yao, Zhen Dong, Amir Gholami, Michael W Mahoney, and Kurt Keutzer. Zeroq: A novel zero shot quantization framework. In *Proceedings of the IEEE/CVF Conference on Computer Vision and Pattern Recognition*, pp. 13169–13178, 2020.

Zhaowei Cai, Xiaodong He, Jian Sun, and Nuno Vasconcelos. Deep learning with low precision by half-wave gaussian quantization. In *Proceedings of the IEEE conference on computer vision and pattern recognition*, pp. 5918–5926, 2017.

Yoni Choukroun, Eli Kravchik, Fan Yang, and Pavel Kisilev. Low-bit quantization of neural networks for efficient inference. In *ICCV Workshops*, pp. 3009–3018, 2019.

Jacob Devlin, Ming-Wei Chang, Kenton Lee, and Kristina Toutanova. Bert: Pre-training of deep bidirectional transformers for language understanding. *arXiv preprint arXiv:1810.04805*, 2018.

Laurent Dinh, Razvan Pascanu, Samy Bengio, and Yoshua Bengio. Sharp minima can generalize for deep nets, 2017.

Zhen Dong, Zhewei Yao, Yaohui Cai, Daiyaan Arfeen, Amir Gholami, Michael W Mahoney, and Kurt Keutzer. Hawq-v2: Hessian aware trace-weighted quantization of neural networks. *arXiv preprint arXiv:1911.03852*, 2019.

Steven K Esser, Jeffrey L McKinstry, Deepika Bablani, Rathinakumar Appuswamy, and Dharmendra S Modha. Learned step size quantization. *arXiv preprint arXiv:1902.08153*, 2019.

Pierre Foret, Ariel Kleiner, Hossein Mobahi, and Behnam Neyshabur. Sharpness-aware minimization for efficiently improving generalization. *arXiv preprint arXiv:2010.01412*, 2020.

Yonggan Fu, Qixuan Yu, Meng Li, Vikas Chandra, and Yingyan Lin. Double-win quant: Aggressively winning robustness of quantized deep neural networks via random precision training and inference. In *International Conference on Machine Learning*, pp. 3492–3504. PMLR, 2021.

Song Han, Huizi Mao, and William J Dally. Deep compression: Compressing deep neural networks with pruning, trained quantization and huffman coding. *arXiv preprint arXiv:1510.00149*, 2015.

Kaiming He, Xiangyu Zhang, Shaoqing Ren, and Jian Sun. Deep residual learning for image recognition. In *Proceedings of the IEEE conference on computer vision and pattern recognition*, pp. 770–778, 2016.

Geoffrey Hinton, Oriol Vinyals, and Jeff Dean. Distilling the knowledge in a neural network. *arXiv preprint arXiv:1503.02531*, 2015.

Sepp Hochreiter and Jürgen Schmidhuber. Flat minima. *Neural computation*, 9(1):1–42, 1997.

Itay Hubara, Yury Nahshan, Yair Hanani, Ron Banner, and Daniel Soudry. Accurate post training quantization with small calibration sets. In *International Conference on Machine Learning*, pp. 4466–4475. PMLR, 2021.

Pavel Izmailov, Dmitrii Podoprikhin, Timur Garipov, Dmitry Vetrov, and Andrew Gordon Wilson. Averaging weights leads to wider optima and better generalization. *arXiv preprint arXiv:1803.05407*, 2018.

Benoit Jacob, Skirmantas Kligys, Bo Chen, Menglong Zhu, Matthew Tang, Andrew Howard, Hartwig Adam, and Dmitry Kalenichenko. Quantization and training of neural networks for efficient integer-arithmetic-only inference. In *Proceedings of the IEEE conference on computer vision and pattern recognition*, pp. 2704–2713, 2018.

Yiding Jiang, Behnam Neyshabur, Hossein Mobahi, Dilip Krishnan, and Samy Bengio. Fantastic generalization measures and where to find them. *arXiv preprint arXiv:1912.02178*, 2019.

Prad Kadambi, Karthikeyan Natesan Ramamurthy, and Visar Berisha. Comparing fisher information regularization with distillation for dnn quantization. 2020.

Nitish Shirish Keskar, Dheevatsa Mudigere, Jorge Nocedal, Mikhail Smelyanskiy, and Ping Tak Peter Tang. On large-batch training for deep learning: Generalization gap and sharp minima. *arXiv preprint arXiv:1609.04836*, 2016.

Alex Krizhevsky, Geoffrey Hinton, et al. Learning multiple layers of features from tiny images. 2009.

Yuhang Li, Ruihao Gong, Xu Tan, Yang Yang, Peng Hu, Qi Zhang, Fengwei Yu, Wei Wang, and Shi Gu. Brecq: Pushing the limit of post-training quantization by block reconstruction. *arXiv preprint arXiv:2102.05426*, 2021a.

Yuhang Li, Feng Zhu, Ruihao Gong, Mingzhu Shen, Xin Dong, Shaoqing Lu, Fengwei Yu, and Shi Gu. Mixmix: All you need for data-free compression are feature and data mixing. In *The IEEE International Conference on Computer Vision (ICCV)*, October 2021b.

Tsung-Yi Lin, Priya Goyal, Ross Girshick, Kaiming He, and Piotr Dollár. Focal loss for dense object detection. In *Proceedings of the IEEE international conference on computer vision*, pp. 2980–2988, 2017.

Christos Louizos, Matthias Reisser, Tijmen Blankevoort, Efstratios Gavves, and Max Welling. Relaxed quantization for discretized neural networks. *arXiv preprint arXiv:1810.01875*, 2018.

Markus Nagel, Rana Ali Amjad, Mart Van Baalen, Christos Louizos, and Tijmen Blankevoort. Up or down? adaptive rounding for post-training quantization. In *International Conference on Machine Learning*, pp. 7197–7206. PMLR, 2020.

Yury Nahshan, Brian Chmiel, Chaim Baskin, Evgenii Zheltonozhskii, Ron Banner, Alex M Bronstein, and Avi Mendelson. Loss aware post-training quantization. *arXiv preprint arXiv:1911.07190*, 2019.

Behnam Neyshabur, Srinadh Bhojanapalli, David McAllester, and Nathan Srebro. Exploring generalization in deep learning, 2017.

Adam Paszke, Sam Gross, Francisco Massa, Adam Lerer, James Bradbury, Gregory Chanan, Trevor Killeen, Zeming Lin, Natalia Gimelshein, Luca Antiga, et al. Pytorch: An imperative style, high-performance deep learning library. *Advances in neural information processing systems*, 32: 8026–8037, 2019.

Haotong Qin, Ruihao Gong, Xianglong Liu, Mingzhu Shen, Ziran Wei, Fengwei Yu, and Jingkuan Song. Forward and backward information retention for accurate binary neural networks. In *The IEEE Conference on Computer Vision and Pattern Recognition (CVPR)*, June 2020.

Ilija Radosavovic, Raj Prateek Kosaraju, Ross Girshick, Kaiming He, and Piotr Dollár. Designing network design spaces. In *Proceedings of the IEEE/CVF Conference on Computer Vision and Pattern Recognition*, pp. 10428–10436, 2020.

Shaoqing Ren, Kaiming He, Ross Girshick, and Jian Sun. Faster r-cnn: Towards real-time object detection with region proposal networks. In *Advances in neural information processing systems*, pp. 91–99, 2015.

Olga Russakovsky, Jia Deng, Hao Su, Jonathan Krause, Sanjeev Satheesh, Sean Ma, Zhiheng Huang, Andrej Karpathy, Aditya Khosla, Michael Bernstein, Alexander C. Berg, and Li Fei-Fei. ImageNet Large Scale Visual Recognition Challenge. *International Journal of Computer Vision (IJCV)*, 115(3):211–252, 2015. doi: 10.1007/s11263-015-0816-y.

Mark Sandler, Andrew Howard, Menglong Zhu, Andrey Zhmoginov, and Liang-Chieh Chen. Mobilenetv2: Inverted residuals and linear bottlenecks. In *Proceedings of the IEEE conference on computer vision and pattern recognition*, pp. 4510–4520, 2018.

Maneet Singh, Mohit Chawla, Richa Singh, Mayank Vatsa, and Rama Chellappa. Disguised faces in the wild 2019. In *Proceedings of the IEEE/CVF International Conference on Computer Vision (ICCV) Workshops*, Oct 2019.

Mingxing Tan, Bo Chen, Ruoming Pang, Vijay Vasudevan, Mark Sandler, Andrew Howard, and Quoc V Le. Mnasnet: Platform-aware neural architecture search for mobile. In *Proceedings of the IEEE Conference on Computer Vision and Pattern Recognition*, pp. 2820–2828, 2019.

Peisong Wang, Qiang Chen, Xiangyu He, and Jian Cheng. Towards accurate post-training network quantization via bit-split and stitching. In *Proc. 37nd Int. Conf. Mach. Learn.(ICML)*, 2020.

Dongxian Wu, Shu-Tao Xia, and Yisen Wang. Adversarial weight perturbation helps robust generalization. *arXiv preprint arXiv:2004.05884*, 2020.

Guandao Yang, Tianyi Zhang, Polina Kirichenko, Junwen Bai, Andrew Gordon Wilson, and Chris De Sa. Swalp: Stochastic weight averaging in low precision training. In *International Conference on Machine Learning*, pp. 7015–7024. PMLR, 2019.

Haichao Yu, Linjie Yang, and Humphrey Shi. Is in-domain data really needed? a pilot study on cross-domain calibration for network quantization. In *Proceedings of the IEEE/CVF Conference on Computer Vision and Pattern Recognition (CVPR) Workshops*, pp. 3043–3052, June 2021.

Ofir Zafrir, Guy Boudoukh, Peter Izsak, and Moshe Wasserblat. Q8bert: Quantized 8bit bert. *arXiv preprint arXiv:1910.06188*, 2019.

Xiangguo Zhang, Haotong Qin, Yifu Ding, Ruihao Gong, Qinghua Yan, Renshuai Tao, Yuhang Li, Fengwei Yu, and Xianglong Liu. Diversifying sample generation for accurate data-free quantization. In *The IEEE Conference on Computer Vision and Pattern Recognition (CVPR)*, June 2021.

Yaowei Zheng, Richong Zhang, and Yongyi Mao. Regularizing neural networks via adversarial model perturbation. In *Proceedings of the IEEE/CVF Conference on Computer Vision and Pattern Recognition*, pp. 8156–8165, 2021.

Barret Zoph and Quoc V Le. Neural architecture search with reinforcement learning. *arXiv preprint arXiv:1611.01578*, 2016.

A Proof of Sec. 4.2

A.1 Part 1

First, we show that quantization could be rewrited for injecting scaled form noise. We assign $a = (k+\lambda)\cdot s, \lambda \in [-0.5, 0.5]$, where k is the round-to-nearest integer in activation quantizer ($k = \lfloor \frac{a}{s} \rceil$). By replacing both sides of the formulation $\hat{a} = (1+u)\cdot a$, the value of u holds:

$$\begin{aligned} k \cdot s &= (1+u)\cdot(k+\lambda)\cdot s \\ u &= \frac{-\lambda}{k+\lambda} \end{aligned} \tag{10}$$

It can be clearly seen that u increases when bits, which restricts the magnitude of k, goes down. And we get the following lemma as many papers (Louizos et al., 2018; Cai et al., 2017) have discussed similarly:

Lemma 2. *The activation quantization noise* $\boldsymbol{u}$ *can be seen as random variables that obey the same distribution in each layer.*

Proof. λ subjects to $\mathcal{U}[-0.5s, 0.5s]$, $k+\lambda = \frac{a}{s}$ obeys some gaussian distribution with step size s ensured per-layer. □

To prove Lemma 1, as the situation of fully connected layers has been clearly presented in Sec. 4.2, we focus on convolution structure, where the activations are matrix and its function is also denoted as ReLU or Identity. Then one layer in the network $\mathcal{G}$ can be interpreted as:

$$\boldsymbol{A}_{i,j}^{(\ell+1)} = f(\boldsymbol{Z}_{i,j}^{(\ell+1)}) = f(\sum_p \sum_q \boldsymbol{A}_{i+p-1,j+q-1}^{(\ell)} \cdot \boldsymbol{W}_{p,q}^{(\ell)}) \tag{11}$$

For clearer clarification, based on $\mathcal{G}$, we construct two networks $\mathcal{G}_1(\hat{\boldsymbol{w}}, \mathbf{1}+\boldsymbol{u})$ and $\mathcal{G}_2(\hat{\boldsymbol{w}} \odot (\mathbf{1}+\boldsymbol{v}))$ on behalf of activation perturbation injection and weight one. Here, we omit $\boldsymbol{x}$ for concision and use the quantized weight for subsequent objective.

Note that $\mathcal{G}_1(\hat{\boldsymbol{w}}, \mathbf{1}+\boldsymbol{u})$ means inserting random variables after each layer's output such that $\boldsymbol{A}_{i,j}^{(\ell)}(1+\boldsymbol{U}_{i,j}^{(\ell)}) = \hat{\boldsymbol{A}}_j^{(\ell+1)}$ and mark its loss as $L(\hat{\boldsymbol{w}}, \mathbf{1}+\boldsymbol{u})$. And model $\mathcal{G}_2(\hat{\boldsymbol{w}} \odot (\mathbf{1}+\boldsymbol{v}))$ means sticking random variables into weight such that $\boldsymbol{Z}_{i,j}^{(\ell+1)} = \sum_p \sum_q \boldsymbol{A}_{i+p-1,j+q-1}^{(\ell)} \cdot \boldsymbol{W}_{p,q}^{(\ell)} \cdot (1+\boldsymbol{V}_{p,q}^{(\ell)})$ and mark its loss as $L(\hat{\boldsymbol{w}} \odot (\mathbf{1}+\boldsymbol{v}))$.

Now, we connect the two networks with Lemma 1, where *the key point is to prove Eq. (6)*:

$$\mathbb{E}\left[L(\hat{\boldsymbol{w}}, \mathbf{1}+\boldsymbol{u}) - L(\boldsymbol{w}, \mathbf{1})\right] \approx \mathbb{E}\left[L(\hat{\boldsymbol{w}}) - L(\boldsymbol{w}) + L(\hat{\boldsymbol{w}} \odot (\mathbf{1}+\boldsymbol{v})) - L(\hat{\boldsymbol{w}})\right] \tag{12}$$

$\mathcal{G}_1(\hat{\boldsymbol{w}}, \mathbf{1}+\boldsymbol{u})$, the quantization model, its optmization objective is defined in the left side of Eq. (12), which could be approximated as below by leveraing Taylor Expansion at $\boldsymbol{u} = \mathbf{0}$:

$$\mathbb{E}\left[L(\hat{\boldsymbol{w}}, \mathbf{1}+\boldsymbol{u}) - L(\boldsymbol{w}, \mathbf{1})\right] \approx \mathbb{E}\left[L(\hat{\boldsymbol{w}}) - L(\boldsymbol{w}) + \boldsymbol{u}^\top \nabla_{\boldsymbol{u}} L(\hat{\boldsymbol{w}}, \mathbf{1})\right] \tag{13}$$

And for $\mathcal{G}_2(\hat{\boldsymbol{w}} \odot (\mathbf{1}+\boldsymbol{v}))$, the flatness of $\hat{\boldsymbol{w}}$ under perturbation $\boldsymbol{v}$, which represents for the last two terms of the right side in Eq. (12), we transform it by Taylor Expansion at $\boldsymbol{v} = \mathbf{0}$ once again:

$$\mathbb{E}\left[L(\hat{\boldsymbol{w}} \odot (\mathbf{1}+\boldsymbol{v})) - L(\hat{\boldsymbol{w}})\right] \approx \mathbb{E}\left[\boldsymbol{v}^\top \nabla_{\boldsymbol{v}} L(\hat{\boldsymbol{w}})\right] \tag{14}$$

Thus, by substituting Eq. (12) by Eq. (13) and Eq. (14), what we need to prove is:

$$\mathbb{E}\left[\boldsymbol{u}^\top \nabla_{\boldsymbol{u}} L(\hat{\boldsymbol{w}}, \mathbf{1})\right] \approx \mathbb{E}\left[\boldsymbol{v}^\top \nabla_{\boldsymbol{v}} L(\hat{\boldsymbol{w}} \odot \mathbf{1})\right] \tag{15}$$

A.2 Part 2

In this part, we demonstrate it by calculating the derivatives with respect to $\boldsymbol{U}_{i,j}$ or $\boldsymbol{V}_{p,q}$ at $\mathbf{0}$ in $\mathcal{G}_1$ and $\mathcal{G}_2$. Note that the activation function satisfies $f(x) = f'(x) \cdot x$, where $f'(\cdot)$ is the derivative.

$$\frac{\partial L(\hat{\boldsymbol{w}}, \mathbf{1})}{\partial \boldsymbol{U}_{i,j}{}^{(\ell+1)}} = \frac{\partial L(\hat{\boldsymbol{w}}, \mathbf{1})}{\partial \hat{\boldsymbol{A}}_{i,j}^{(\ell+1)}} \cdot \boldsymbol{A}_{i,j}^{(\ell+1)} = \frac{\partial L(\boldsymbol{w}, \mathbf{1})}{\partial \hat{\boldsymbol{A}}_{i,j}^{(\ell+1)}} \cdot f(\sum_p \sum_q \hat{\boldsymbol{A}}_{i+p-1,j+q-1}^{\ell} \cdot \boldsymbol{W}_{p,q}^{\ell}) \tag{16}$$

$$\begin{aligned} \frac{\partial L(\hat{\boldsymbol{w}}, \mathbf{1})}{\partial \boldsymbol{U}_{i,j}{}^{(\ell+1)}}\Big|_{\boldsymbol{U}=\mathbf{0}} &= \frac{\partial L(\hat{\boldsymbol{w}}, \mathbf{1})}{\partial \boldsymbol{A}_{i,j}^{(\ell+1)}}\Big|_{\boldsymbol{U}=\mathbf{0}} \cdot f(\sum_p \sum_q \boldsymbol{A}_{i+p-1,j+q-1}^{(\ell)} \cdot \boldsymbol{W}_{p,q}^{(\ell)}) \\ &= \sum_p \sum_q \underbrace{\frac{\partial L(\hat{\boldsymbol{w}}, \mathbf{1})}{\partial \boldsymbol{A}_{i,j}^{(\ell+1)}}\Big|_{\boldsymbol{U}=\mathbf{0}}}_{(1)} \cdot \underbrace{f'(\boldsymbol{Z}_{i,j}^{(\ell+1)}) \cdot \boldsymbol{A}_{i+p-1,j+q-1}^{(\ell)} \cdot \boldsymbol{W}_{p,q}^{(\ell)}}_{(2)} \end{aligned} \tag{17}$$

$$\begin{aligned} \frac{\partial L(\hat{\boldsymbol{w}} \odot \mathbf{1})}{\partial \boldsymbol{V}_{p,q}{}^{(\ell)}}\Big|_{\boldsymbol{V}=\mathbf{0}} &= \sum_i \sum_j \frac{\partial L(\hat{\boldsymbol{w}} \odot \mathbf{1})}{\partial \boldsymbol{A}_{i,j}^{(\ell+1)}}\Big|_{\boldsymbol{V}=\mathbf{0}} \cdot f'(\boldsymbol{Z}_{i,j}^{(\ell+1)}) \cdot \frac{\partial \boldsymbol{Z}_{i,j}^{(\ell+1)}}{\partial \boldsymbol{V}_{p,q}^{(\ell)}} \\ &= \sum_i \sum_j \underbrace{\frac{\partial L(\hat{\boldsymbol{w}} \odot \mathbf{1})}{\partial \boldsymbol{A}_{i,j}^{(\ell+1)}}\Big|_{\boldsymbol{V}=\mathbf{0}}}_{(1)} \cdot \underbrace{f'(\boldsymbol{Z}_{i,j}^{(\ell+1)}) \cdot \boldsymbol{A}_{i+p-1,j+q-1}^{\ell} \cdot \boldsymbol{W}_{p,q}^{(\ell)}}_{(2)} \end{aligned} \tag{18}$$

Eq. (17) defines the derivative to $\boldsymbol{U}_{i,j}^{\ell+1}$ while Eq. (17) defines the derivative to $\boldsymbol{V}_{i,j}^{\ell}$. Assuming the two networks take the same weight $\hat{\boldsymbol{w}}$ thus the same activation with zero $\boldsymbol{v}$ and $\boldsymbol{u}$ and $\frac{\partial L(\hat{\boldsymbol{w}}, \mathbf{1})}{\partial \boldsymbol{A}_{i,j}^{(\ell+1)}}\Big|_{\boldsymbol{U}=\mathbf{0}}$ equals to $\frac{\partial L(\hat{\boldsymbol{w}} \odot \mathbf{1})}{\partial \boldsymbol{A}_{i,j}^{(\ell+1)}}\Big|_{\boldsymbol{V}=\mathbf{0}}$. Then Eq. (17) calculates others by summing term (2) where the weight $\boldsymbol{W}_{p,q}^{\ell}$ denotes the connection ending at $\boldsymbol{A}_{i,j}^{\ell+1}(\boldsymbol{U}_{i,j}^{\ell+1})$. Eq. (18) also calculates the same term, where $\boldsymbol{A}_{i,j}^{\ell+1}$ denotes the neurons that $\boldsymbol{W}_{p,q}^{\ell}$ connects with.

A.3 PART 3

We demonstrate the Eq. (15) by the illustration above.

$$\begin{aligned}
\mathbb{E}[\boldsymbol{u}^\top \nabla_{\boldsymbol{u}} L(\hat{\boldsymbol{w}}, \mathbf{1})] &= \mathbb{E}\left[\sum_{\ell}\sum_{i}\sum_{j} \boldsymbol{U}_{i,j}^{(\ell)} \cdot \frac{\partial L(\hat{\boldsymbol{w}}, \mathbf{1})}{\partial \boldsymbol{U}_{i,j}{}^{(\ell)}}\right] \\
&\overset{(1)}{\approx} \sum_{(\ell)}\sum_{i}\sum_{j} \mathbb{E}\left[\boldsymbol{U}_{i,j}^{(\ell)}\right] \cdot \mathbb{E}\left[\frac{\partial L(\hat{\boldsymbol{w}}, \mathbf{1})}{\partial \boldsymbol{U}_{i,j}{}^{(\ell)}}\right] \\
&\overset{(2)}{\approx} \sum_{(\ell)}\sum_{i}\sum_{j} \mathbb{E}\left[\boldsymbol{U}^{(\ell)}\right] \cdot \mathbb{E}\left[\frac{\partial L(\hat{\boldsymbol{w}}, \mathbf{1})}{\partial \boldsymbol{U}_{i,j}{}^{(\ell)}}\right]
\end{aligned} \tag{19}$$

For (1), we assume the two variables inside the expectation are independent since $\boldsymbol{U}$ will not be updated by the derivative directly. For (2), according to Lemma 2, quantization noise can be seen as random variables which obeys the same distribution in one layer such that $\mathbb{E}\left[\boldsymbol{U}_{i,j}^{(\ell)}\right] = \mathbb{E}\left[\boldsymbol{U}^{(\ell)}\right]$. By substituting Eq. (17) into the above formulation, we have:

$$\begin{aligned}
\mathbb{E}[\boldsymbol{u}^\top \nabla_{\boldsymbol{u}} L(\hat{\boldsymbol{w}}, \mathbf{1})] &\approx \sum_{\ell} \mathbb{E}\left[\boldsymbol{U}^{(\ell)}\right] \sum_{i,j}\sum_{p,q} \mathbb{E}\left[T\right] \\
&= \sum_{(\ell)} \mathbb{E}\left[\boldsymbol{U}^{(\ell)}\right] \sum_{p,q}\sum_{i,j} \mathbb{E}\left[T\right]
\end{aligned} \tag{20}$$

where

$$\begin{aligned}
T &= \frac{\partial L(\hat{\boldsymbol{w}} \odot \mathbf{1})}{\partial \boldsymbol{A}_{i,j}^{(\ell+1)}}\Big|_{\boldsymbol{U}=\mathbf{0}} \cdot f'(\boldsymbol{Z}_{i,j}^{(\ell+1)}) \cdot \boldsymbol{A}_{i+p-1,j+q-1}^{\ell} \cdot \boldsymbol{W}_{p,q}^{(\ell)} \\
&= \frac{\partial L(\hat{\boldsymbol{w}} \odot \mathbf{1})}{\partial \boldsymbol{A}_{i,j}^{(\ell+1)}}\Big|_{\boldsymbol{V}=\mathbf{0}} \cdot f'(\boldsymbol{Z}_{i,j}^{(\ell+1)}) \cdot \boldsymbol{A}_{i+p-1,j+q-1}^{\ell} \cdot \boldsymbol{W}_{p,q}^{(\ell)}
\end{aligned} \tag{21}$$

Now, it can be clearly observed that by constructing weight perturbation $\boldsymbol{V}$ that $\mathbb{E}[\boldsymbol{V}_{i,j}^{(\ell)}] = \mathbb{E}[\boldsymbol{V}^{(\ell)}] = \mathbb{E}[\boldsymbol{U}^{(\ell)}]$ each layer, the following fomulation satisfies.

$$\begin{aligned}
\mathbb{E}[\boldsymbol{u}^\top \nabla_{\boldsymbol{u}} L(\hat{\boldsymbol{w}}, \mathbf{1})] &\approx \sum_{\ell} \mathbb{E}\left[\boldsymbol{V}^{(\ell)}\right] \sum_{p,q}\sum_{i,j} \mathbb{E}\left[T\right] \\
&\approx \sum_{(\ell)}\sum_{p,q}\sum_{i,j} \mathbb{E}\left[\boldsymbol{V}_{i,j}^{(\ell)}\right] \cdot \mathbb{E}\left[T\right] \\
&\approx \mathbb{E}\left[\sum_{\ell}\sum_{p}\sum_{q} \boldsymbol{V}_{p,q}^{(\ell)} \cdot \frac{\partial L(\hat{\boldsymbol{w}} \odot \mathbf{1})}{\partial \boldsymbol{V}_{i,j}{}^{(\ell)}}\right] \\
&\approx \mathbb{E}\left[\boldsymbol{v}^\top \nabla_{\boldsymbol{v}} L(\hat{\boldsymbol{w}} \odot \mathbf{1})\right]
\end{aligned} \tag{22}$$

Therefore, Eq. (15) has been proved thus the demonstration of Eq. (12) and Lemma 1 is available.

B EXPERIMENTS

B.1 SUPPLEMENTARY EXPERIMENTS OF SEC. 4.1

To further illustrate that different optimization weight is the key point for accuracy of post-training quantization, we conduct some ablation studies that replacing activation quantization or weight one with setting in quantization-aware training, which usually behaves well, respectively.

In detail, by altering the activation quantization with QAT training, we use the whole ImageNet and the LSQ (Esser et al., 2019) scheme to learn the step size of activation for 5 epochs. And for weight one, we still keep rounding up or down strategy, which is adopted in PTQ but with the whole training set and 40 optimization epochs.

Method	Bits (W/A)	ResNet-18	SWA_{20}
	FP32	71.058	**71.502**
Min-Max*	8/8	70.938	**71.402**
	4/8	52.326	**65.264**
	4/4	26.052	**44.368**
OMSE (Choukroun et al., 2019)*	4/4	38.318	**55.860**
	32/4	64.146	**65.990**
BRECQ (Li et al., 2021a)*	2/4	65.350	**66.334**
	2/2	41.740	**44.304**

However, results in Table 7 are surprising that although the optimization space in weight is kept very restricted, leveraging the whole data to implement weight tuning can achieve a large accuracy boost. And the activation quantization step size might not be as important as weight. These findings indicate that exploring a quantization-friendly weight may be the fresh insight for accurate post-training quantization, where this work dedicates to. In the next part, we will further discuss about it from a flatness perspective.

B.2 Flatness and Post-Training Quantization

While there are plenty of works exploring the correlation between flatness and generalization and devoting to fruitful techniques to achieve a better loss landscape, the interaction between quantization and flatness has not been exploited much. In this paper, we first connect flatter weight with activation quantization from PTQ view, as implied in Sec. 4.2. From this, we conjecture that flatness and quantization might be helpful to each other.

By leveraging some mechanisms such as (Izmailov et al., 2018; Foret et al., 2020), FP32 models with smoother loss surface are adopted to validate the performance on quantization compared with the naive one.

In Table **??**, model SWA_{20} is enabled by applying the SWA trick (Izmailov et al., 2018) to ResNet-18 and finetuned 20 epochs on the whole ImageNet. From the table, the observation is that the promotion about generalization can not fully reveal the enhancement induced by SWA about quantization. With even lower bits thus larger noise, SWA_{20} surpasses the naive one by a large margin.

The above experimental results imply that distinct FP32 models with analogous accuracy might contribute to surprisingly disparate outcomes after PTQ, especially for those naive mechanisms without any weight tuning.

In turn, there have been some studies that delve into robustness boost by applying quantization. (Fu et al., 2021) advocates that quantization can be properly leveraged to enhance DNNs' robustness, even beyond their full-precision counterparts. They propose a random bit training strategy to accomplish it, which our work illustrates the correlation with bit and perturbation in Sec. A.1.

B.3 Other choices for perturbation type

Rethinking Sec. 4.3, there are numerous tricks to promote the flatness on the test set, such as using data augmentation for diverse $\boldsymbol{x}$, modifying $\boldsymbol{v}(\boldsymbol{x})$ directly even like (Foret et al., 2020), which injects the worst-case weight perturbations or adjusting $\boldsymbol{u}(\boldsymbol{x})$ to acquire $\boldsymbol{v}(\boldsymbol{x})$ from another distribution.

In this part, we inspect other strategies and discover that they all cause some performance drop to some extent except the data augmentation trick. We hypothesis that it is made by increasing the objective loss described in Eq. (4), where for asymmetric weight reconstruction, the increased weird loss in one block induced by employing these tricks will be amplified to subsequent ones and lead to a failure. However, our method, which tries to drop some quantiza-

Algorithm 2: Implementations of three cases in Sec. 4.1

Input: Model with K blocks.
if *Case 2* **then**
  for $k = 1$ *to* K **do**
    parameterize activation step size in this block ;
for $k = 1$ *to* K **do**
  Tuning weight like (Li et al., 2021a) by reconstructing block output ;
  if *Case 3* **then**
    parameterize activation step size in this block ;
if *Case 1* **then**
  for $k = 1$ *to* K **do**
    parameterize activation step size in this block ;
return Quantized model ;

tion and keep it in FP32 signal, masks some reconstruction loss thereby has no such worries.

Activation setting	Weight setting	Accuracy
PTQ	PTQ	51.19
QAT	PTQ	52.84
PTQ	QAT	**58.93**

Table 7: Ablation study of quantization settings on ResNet-18 W2A2

Methods	Accuracy
Baseline	51.19
Stochastic Round	48.49
SAM (Foret et al., 2020)	50.05
Data Augmentation	**51.87**
QDROP (Ours)	**54.72**

Table 8: Impact of different design choices for Sec. 4.3, with W2A2 on ImageNet and ResNet-18

C IMPLEMENTATION DETAILS

Observation. Here, we give the concrete implementation of experiments in Sec. 4.1. We actually consider three ways of introducing activation for Case 2, but we find the difference of outcomes among them are negligible thus employing one of them for clearer clarification.

ImageNet. We extract 1024 training examples from ImageNet dataset as calibration dataset based on the standard pre-process. Pretrain-models are downloaded from BRECQ's open source code. Hyper-parameters we keep it as BRECQ, such as set batch size 32, learning rate for activation step size 4e-5, learning rate for weight tuning 1e-3, iterations 2x104. Following BRECQ, we first fold batch normalization layer into convolution before tuning the weight then reconstruct output block-wise, where we tune the weight by rounding up or down, use LSQ (Esser et al., 2019)to parameterize activation step size. As for our extra content, we learn the weight and activation parameters together and use 50% rate to drop some activation quantization.

Object detection. Here, we also obey BRECQ' setting and use the same pretrain-models with 256 training samples taken from MS COCO dataset for calibration. Parameters about resolution is set to 800 (max size 1333) and 600 (max size 1000) for ResNets and MobileNetV2, respectively and batch size is set to 2 while others are the same as classification task. To be noted, we didn't quantize the head with applying block reconstruction to backbone and layer reconstruction to neck like BRECQ.

GLUE benchmark and SQuAD. The BERT fine-tuned models are taken from huggingface group (https://huggingface.co/). And we sampled 1024 examples from training set. We keep the maximum sequence length to be 128 for GLUE benchmark but maximum sequence length 384 with doc stride 128 for SQuAD1.1, which is the usual choice. Also, we quantize all the part in BERT as well as the internal structure of the attention module with only affirming the embedding weight to 8-bit. Other settings and hyper-parameters are chosen in the same way as ImageNet experiments.

Baselines. We run baseline methods from open-source codes, such as AdaQuant (Hubara et al., 2020), BRECQ and Adaround. And we try our best to align some optimal settings like per-channel quantization for fair comparisons.